Available online at www.sciencedirect.com
ScienceDirect
Journal of Power Sources 162 (2006) 279–285
JOURNAL OF POWER SOURCES
www.elsevier.com/locate/jpowsour

Preparation and properties of ceramic interconnecting materials, $La_{0.7}Ca_{0.3}CrO_{3-\delta}$ doped with GDC for IT-SOFCs

Xiaoliang Zhou, Jianjun Ma, Feijun Deng, Guangyao Meng, Xingqin Liu *

Department of Materials Science and Engineering, University of Science and Technology of China, Hefei, Anhui 230026, PR China

Received 23 May 2006; received in revised form 21 June 2006; accepted 21 June 2006
Available online 23 August 2006

Abstract

One of the challenges for improving the performance and cost-effectiveness of solid oxide fuel cells (SOFCs) is the development of effective interconnect materials. A widely used interconnect ceramic for SOFCs is doped lanthanum chromite. In this paper, we report a doped lanthanum chromite, $La_{0.7}Ca_{0.3}CrO_{3-\delta}$ (LCC) + x wt.% $Gd_{0.2}Ce_{0.8}O_{1.9}$ (GDC) (x = 0–10), with improved electrical conductivity and sintering capability. In this composite material system, LCC + GDC were prepared by an auto-ignition process and the electrical conductivity was characterized in air and in H_2. The LCC powders exhibited a better sintering ability and could reach a 94.7% relative density at 1400 °C for 4 h in air and with the increase of GDC content the relative density increased, reached 98.5% when the GDC content was up to 10 wt.%. The electrical conductivity of the samples dramatically increased with GDC addition until a maximum of 134.48 S cm^{-1} in air at 900 °C when the materials contained 3 wt.% GDC. This is 5.5 times higher than pure LCC (24.63 S cm^{-1}). For the sample with a 1 wt.% GDC content, the conductivity in pure H_2 at 900 °C was a maximum 5.45 S cm^{-1}, which is also higher than that of pure LCC ceramics (4.72 S cm^{-1}). The average thermal expansion coefficient (TEC) increased with the increase of GDC content, ranging from 11.12 to 14.32 × 10^{-6} K^{-1}, the majority of which unfortunately did not match that of 8YSZ. The oxygen permeation measurement presented a negligible oxygen ionic conduction, indicating that it is still an electronically conducting ceramic. Therefore, it is a very promising interconnect material for higher performance and cost-effectiveness for SOFCs.

PACS: Fuel cell (84.60 D)

Keywords: $La_{0.7}Ca_{0.3}CrO_3$; Auto-ignition process; Electrical conductivity; Interconnect; SOFC

1. Introduction

Solid oxide fuel cells (SOFCs) are promising, clean and efficient power sources and have been the subject of intensive research and development over the past two decades because of their high efficiency of energy conversion and the variety of acceptable fuels and their long-term stability [1–4]. Lanthanum chromite ($LaCrO_3$)-based perovskite materials were widely studied as the ceramic interconnect for SOFCs owing to their thermal and chemical stability and high electrical conductivity at both reducing and oxidizing atmospheres [4–6]. However, there are still several problems to be solved such as poor sinterability in air resulting from the volatilization of chromium, an unmatched thermal expansion coefficient (TEC) with that of other components of the SOFC and insufficiently high conductivity. In recent years, many efforts have been devoted to the study of lanthanum chromites by doping alkaline metals or transition metals at La-site or Cr-site [7–10]. Alkaline metals were conventionally doped at the La-site of $LaCrO_3$ and transition metals at the Cr-site. Weber et al. reported that the substitution of divalent Ca and Sr for Y and La, respectively, induced the formation of small polarons as charge carriers whereas the additional substitution of Mn for Cr resulted in the formation of a second charge carrier associated with Mn [10]. Mori et al. [8] have found that Co-doped $La_{0.9}Sr_{0.1}CrO_3$-based perovskites synthesized by the Pechini method exhibited excellent sintering characteristics in air–$La_{0.9}Sr_{0.1}Cr_{0.95}Al_{0.02}Co_{0.02}O_3$ presented linear thermal expansion behavior and its TEC was in good agreement with that of 8 mol%-Y_2O_3-stabilized-ZrO_2 (YSZ) electrolyte. To develop a new kind of interconnect material with superior electrical prop-

* Corresponding author. Tel.: +86 551 3603249; fax: +86 551 3607627.
E-mail address: tianliangzhou@sina.com (X. Liu).

0378-7753/$ – see front matter © 2006 Elsevier B.V. All rights reserved.
doi:10.1016/j.jpowsour.2006.06.091

erties for IT-SOFCs, the perovskite-type materials have been widely studied on account of their unique electronic conductivity [11]. However, little work has been done on the material system of LCC ($La_{0.7}Ca_{0.3}CrO_{3-\delta}$) with introduction of GDC ($Gd_{0.2}Ce_{0.8}O_{1.9}$).

Wet chemical processes, such as hydrothermal synthesis and homogeneous precipitation [12,13], have been applied to prepare fine doped-ceria powders with good sinterability. Recently, the glycine-nitrate process (GNP) has been introduced as one of a general class of combustion methods for the preparation of ceramic powders [14]. GNP is a relatively inexpensive preparation technique to produce fine, homogeneous powders and has been used to prepare simple oxides as well as multi-component oxides successfully [15–17]. The auto-ignition process is a self-combustion method using citric acid as the fuel and nitrates of the metal components of the target material as oxidants. This procedure could enhance the density and phase purity of the sample at lower temperature. In this study, we used GNP and an auto-ignition process to synthesize GDC powder and obtain highly active LCC powders, respectively. LCC and GDC powders were then compacted to produce the dense materials, which could be fabricated without any control of oxygen pressure. The thermal expansion, sintering characteristics, crystal structure and electrical conductivity of the composite LCC/GDC were then investigated to evaluate its application as an interconnect materials for IT-SOFCs.

2. Experimental

Fine powders of $La_{0.7}Ca_{0.3}CrO_{3-\delta}$ were synthesized by an auto-ignition process. The starting materials, calcium nitrate ($Ca(NO_3)_2{\cdot}4H_2O$) (AR), lanthanum oxide (La_2O_3) (AR) and chromic nitrate ($Cr(NO_3)_3{\cdot}6H_2O$) (AR), were mixed with three times as much citric acid in distilled water. The mixture was then heated to form a gel and the wet gel was further heated to about 120 °C to remove the solvents. The dried gel was placed in an oven at 650 °C. The combustion reaction took place within a few seconds, forming the primary powder. The as-synthesized powders were calcined at 650 °C for 2 h.

In order to prepare $Gd_{0.2}Ce_{0.8}O_{1.9}$ (GDC) powders by GNP, stoichiometric amounts of $Ce(NO_3)_3{\cdot}6H_2O$ (AR) and $Gd(NO_3)_3{\cdot}6H_2O$ (AR) were dissolved in distilled water and 1.2 mol of glycine was added per mole of nitrate. After spontaneous ignition, the resulting pale-yellow ash was collected and calcined in air at 600 °C for 2 h to remove any carbon residue remaining in the oxide powder, and a well-crystalline structure was formed.

The fine powders with the composition of LCC + x wt.% GDC (x = 0, 1, 2, 3, 4, 5, 6, 8 and 10) were ball-milled in an ethanol medium overnight and dried subsequently. Small pellets and rectangular bar specimens were then produced by pressing at 360 MPa and sintering in air at 1400 °C for 4 h. The heating rate was fixed at 1 °C min^{-1} before 550 °C and 2 °C min^{-1} between 550 and 1400 °C.

Particle size and fractured surfaces of the sintered specimens were observed by scanning electron microscopy (Hitachi X-650 and XT30 ESEM-TMP). Various phases of the sintered samples were identified by X-ray diffraction analysis on a Philips PW 1730 diffractometer using Cu Kα radiation. The electrical conductivity of the materials was studied from 450 to 900 °C using a standard dc four-probe technique on a H.P. multimeter (Model 34401). Rectangular bar specimens were used for this purpose. The thermal expansion was measured at 30–1000 °C on cylindrical rods of the sintered samples using a dilatometer (SHIMADZU50) at a heating rate of 5 °C min^{-1}. The oxygen penetration flux was measured by gas chromatography.

3. Experimental results

3.1. XRD phase structure analysis

The XRD patterns of GDC and LCC + x wt.% GDC (x = 0, 2, 4, 6, 8, 10) obtained after sintered at the temperature of 1400 °C for 4 h are shown in Fig. 1. The XRD pattern of the GDC sample displayed all peaks associated with a pure fluorite structure. The LCC sample showed a pure perovskite phase with an orthorhombic symmetry and no other phases were observed. For other samples, as shown in Fig. 1, LCC and GDC still remained after sintering at 1400 °C for 4 h. Thus, in consideration of XRD, it may be concluded that there was no second phase even at 1400 °C. However, it is possible that a portion of the GDC dissolved into the LCC structure since XRD commonly has a detection limit of ~5%.

3.2. SEM analysis and relative density measurements

The SEM images of the samples for the selected sintering conditions (Fig. 2) showed that dense materials were fabricated in air after sintering, suggesting that the present powders were sinterable. Clear grain boundaries were observed, along which the grains grew perfectly straight. This feature of the microstructure usually appears in a densely sintered body. The average grain sizes were determined by direct observation. As shown in Fig. 2, the average grain sizes of the different samples ranged from 3 to 7 μm. Fig. 2a showed that the average grain size was 7 μm when the sample contained no GDC. The average grain

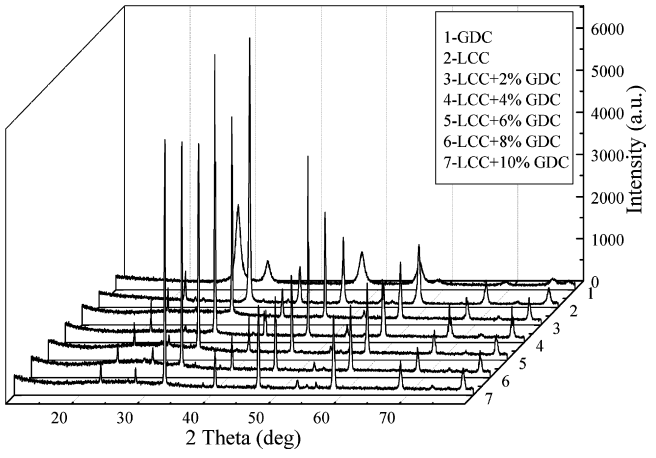

Fig. 1. X-ray diffraction patterns of GDC and LCC + x wt.% GDC (x = 0, 2, 4, 6, 8, 10) obtained after sintering at 1400 °C for 4 h.

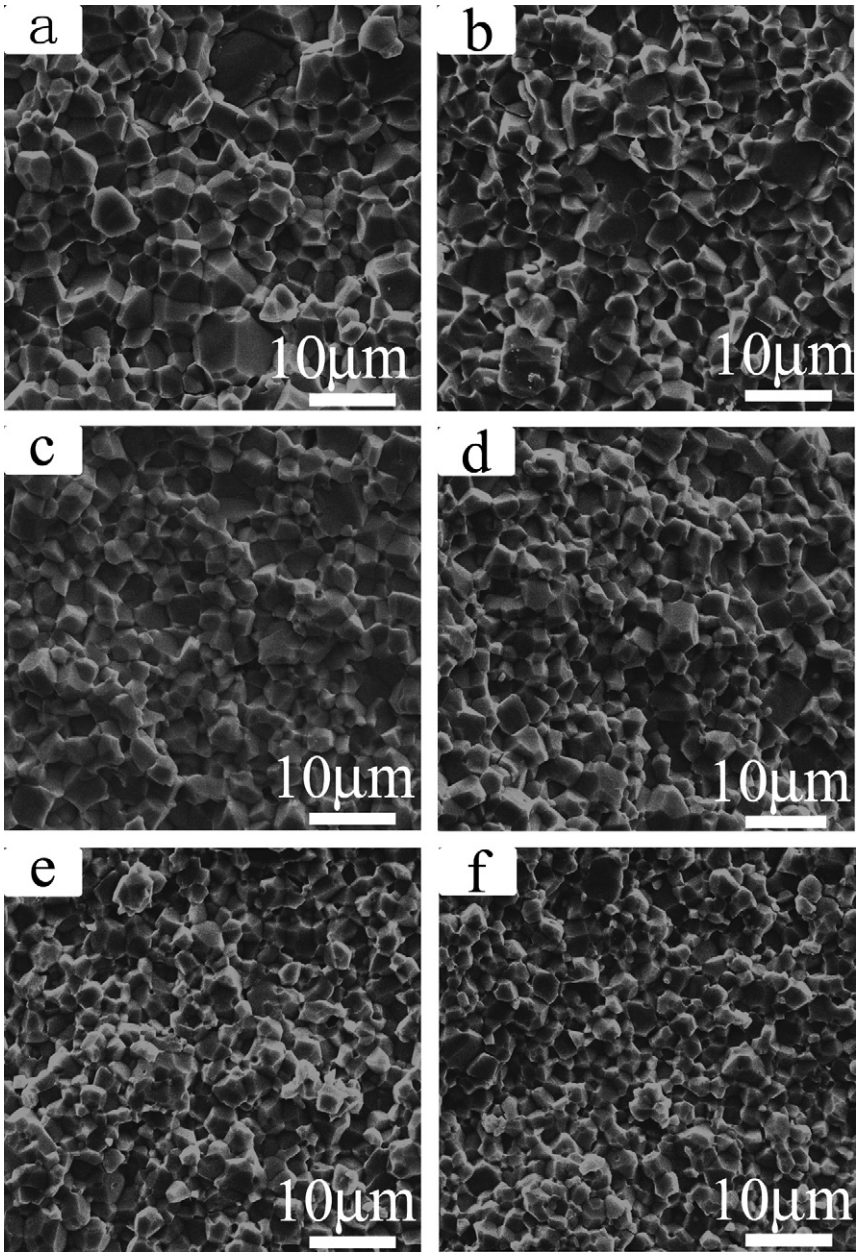

Fig. 2. The SEM images of the samples sintered at 1400 °C for 4 h: panels a–f show LCC + 0 wt.% GDC, LCC + 2 wt.% GDC, LCC + 4 wt.% GDC, LCC + 6 wt.% GDC, LCC + 8 wt.% GDC and LCC + 10 wt.% GDC, respectively.

sizes of the other samples were smaller than that of the sample without GDC, and with the increase of GDC content the average grain size decreased. The existence of GDC thus restrained the growth of grains. The influence of the GDC content on the relative density of different LCC + GDC samples is shown in Fig. 3. With the increase of GDC content from 0 to 10 wt.%, the relative density increased from 94.7% to 98.5%. Therefore, GDC served as an effective sintering aid in enhancing the sinterability of the powders.

3.3. Electrical conductivity

The electrical conductivity of this material system was characterized both in air and in H_2. Figs. 4 and 5 show the effects of temperature and the GDC content on the electrical conductivity in air. The samples containing different GDC contents, ranging from 0 to 10 wt.%, were investigated at different temperatures in air. In Fig. 4, it can be seen that the electrical conductivities of the samples with a specific GDC content increased with increasing temperature and reached a maximum at 900 °C. At each specific temperature studied, the electrical conductivities of the samples reached a maximum when the sample contained 3 wt.% GDC. Therefore, the sample with 3 wt.% GDC had the maximum conductivity of 134.48 S cm^{-1} at 900 °C under these experimental conditions. This is about 5.5 times as high as that of the commonly used lanthanum chromite ($La_{0.7}Ca_{0.3}CrO_3$) (24.63 S cm^{-1}). It is worthy to note that even at a temperature of 700 and 800 °C, the electrical conductivities reached 112.84

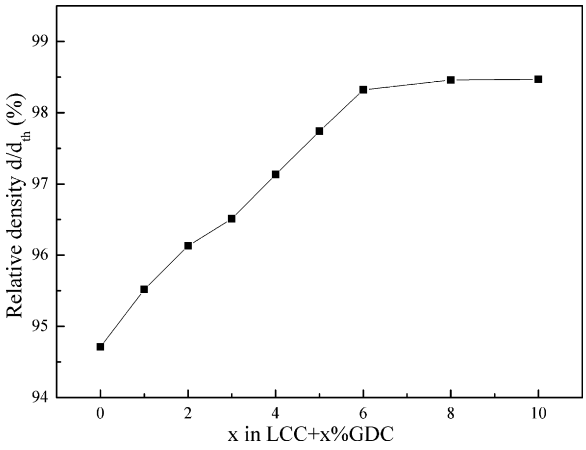

Fig. 3. The influence of the GDC content in LCC + GDC on the relative density of different samples.

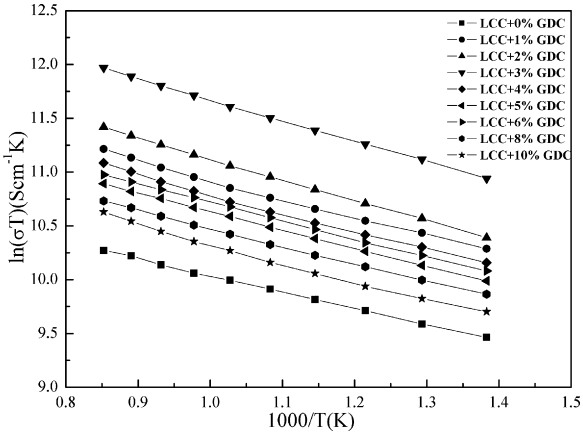

Fig. 4. Arrhenius plots of the conductivities for the samples with different GDC contents in air.

and 124.56 S cm^{-1}, respectively. Fig. 5 shows the effects of the GDC content on the conductivity of the samples in air at various temperatures. The electrical conductivity dramatically increased with increasing GDC content up to 3 wt.% in air. Interestingly, a sudden change in electrical conductivity occurred as the GDC content was further increased. Indeed, when the GDC contents increased from 0 to 3 wt.%, the electrical conductivities increased rapidly to the maximum, and then dropped as the GDC content increased to 4 wt.%, showing a sharper change than that of the samples with GDC contents ranging from 4 to 10 wt.%. Compared with temperature, a lower GDC content (<4 wt.%) can affect the electrical conductivities dramatically, suggesting that GDC played a more important role in determining the conductivity of this materials system.

Arrhenius plots of conductivities for the samples with different GDC contents in pure H_2 are shown in Fig. 6. The electrical conductivities of the samples increased with increasing temperature. At 900 °C, the electrical conductivity reached the maximum. The sample containing 1 wt.% GDC has a maximum electrical conductivity of 5.45 S cm^{-1} which is also higher than that of the pure LCC ceramics (4.72 S cm^{-1}).

As shown in Fig. 4, all the LCC + GDC ceramics displayed linear conductivity behavior in the temperature range from 723 to 1173 K. The linear relationship between ln(σT) and 1/T indicates that the electrical conductivity behavior obeys the small polaron conductivity mechanism, as expressed in the following equation

$$\sigma = \frac{A}{T}\exp\left(-\frac{E_a}{kT}\right) \quad (1)$$

where A is a pre-exponential factor, k the Boltzmann constant, T the absolute temperature, and E_a is the activation energy for the conduction. All the data are in agreement with the linear behavior predicted in Eq. (1), suggesting that the conductivity is a thermally activated process associated with a temperature-independent carrier concentration [10]. An earlier study [18] on $LaCrO_3$ indicated that it was a p-type conductor and became non-stoichiometric through the formation of cation vacancies. The negatively charged cation vacancies were electrically compensated by the concomitant appearance of positively charged electron holes. Electrical conduction in the undoped $LaCrO_3$ occurred by the small polaron mechanism via transport of electron holes. The p-type non-stoichiometric reaction is given by

$$\tfrac{3}{2}O_2 \leftrightarrow V'''_{La} + V'''_{Cr} + 3O_O{}^{\times} + 6h^{\bullet} \quad (2)$$

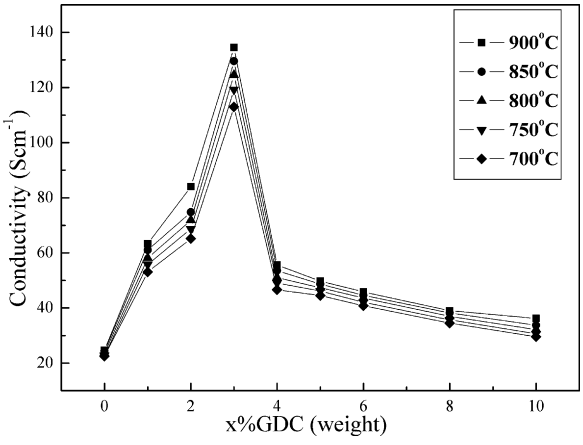

Fig. 5. Effect of the GDC content on the conductivity of the samples in air at various temperatures.

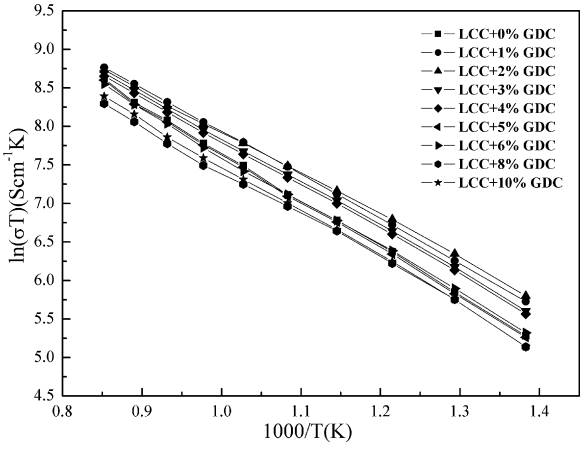

Fig. 6. Arrhenius plots of the conductivities for the samples with different GDC contents in pure H_2.

where V'''_{La} and V'''_{Cr} refers to La and Cr vacancy, respectively, $O_O{}^{\times}$ the oxygen site, and $h^{\bullet}$ is the electron hole. In order to improve the electrical conductivity and TEC, $LaCrO_3$ is often doped at lanthanum or chromium or both sites of perovskite structure for practical application. Because of the ionic radius similarity, strontium and calcium tend to replace La ions whereas magnesium, iron, nickel, copper and cobalt take over Cr ions.

A number of articles [18–27] have addressed the nature of the defect chemistry and electrical conductivity of doped $LaCrO_3$. It is well documented that in a high oxygen activity environment where oxygen partial pressure is typically larger than 10^{-8} atm, the negatively charged M'_{LA} (M refers to Sr or Ca) or N'_{Cr} (N represents Mg, Fe, Ni, Cu, or Co) is electronically compensated by a $Cr^{3+} \rightarrow Cr^{4+}$ transition. The neutrality condition can be simply described as

$$\left[M'_{La}\right] \text{ or } \left[N'_{Cr}\right] = [Cr_{Cr}{}^{\bullet}] \quad (3)$$

where [ ] indicates concentration, $Cr_{Cr}{}^{\bullet}$ is Cr^{4+} in Cr-site. In the case of $La_{1-x}Ca_xCrO_3$, Eq. (3) becomes $\left[Ca'_{La}\right] = [Cr_{Cr}{}^{\bullet}]$. The predominant defect species are considered to be Ca'_{La} and $Cr_{Cr}{}^{\bullet}$, invoking the Kroger–Vink notion. The electrical transport in doped $LaCrO_3$ is dominated by small-polaron hopping of charge carrier localized at the Cr-sites. In this situation, the notions of $h^{\bullet}$ and $Cr_{Cr}{}^{\bullet}$ have the same implication.

In low oxygen activity regime, the equilibrium between the defect species and the surrounding atmosphere is expressed by

$$\tfrac{1}{2}O_2 + V_O{}^{\bullet\bullet} + 2Cr_{Cr}{}^{\times} \leftrightarrow O_O{}^{\times} + 2Cr_{Cr}{}^{\bullet} \quad (4)$$

where $Cr_{Cr}{}^{\times}$ represents Cr-site and $V^{\bullet\bullet}$ is oxygen vacancy. To maintain electroneutrality in the whole crystal, the following equation must be held

$$\left[M'_{La}\right] \text{ or } \left[N'_{Cr}\right] = 2\,[V_O{}^{\bullet\bullet}] + [Cr_{Cr}{}^{\bullet}] \quad (5)$$

This means that under reducing conditions, the lattice oxygen transforms into a doubly charged oxygen vacancy consuming two electron holes simultaneously. The charge imbalance caused by the introduction of aliovalent dopants is compensated by the formation of the oxygen vacancy.

For Ca-doped $LaCrO_3$, $La_{1-x}Ca_xCrO_3$ should be expressed as $La_{1-x}Ca_xCrO_{3-\delta}$ due to the presence of oxygen vacancies (Eq. (5)) becomes

$$\left[Ca'_{La}\right] = 2\,[V_O{}^{\bullet\bullet}] + [Cr_{Cr}{}^{\bullet}] \quad (6)$$

Under an oxidizing atmosphere such as oxygen or air at the cathode where the oxygen partial pressure is relatively high ($10^{-0.7}$ to 10^{-4} atm), the conductivity is enhanced on account of the induced Cr^{3+} to Cr^{4+} transition via an electronic compensation mechanism. On the other hand, in a reducing environment such as in fuel gases, at the anode where the oxygen partial pressure is low (10^{-8} to 10^{-18} atm), the conductivity is appreciably retarded due to the appearance of oxygen vacancies via the ionic compensation mechanism [28]. For Ca-doped $LaCrO_3$, $La_{1-x}Ca_xCrO_3$, higher doping levels contribute to a larger electrical conductivity, owing to the higher concentration of electron holes. The different electrical conductivity behaviors are demonstrated in Figs. 5–8. From Fig. 5, it can be observed that the

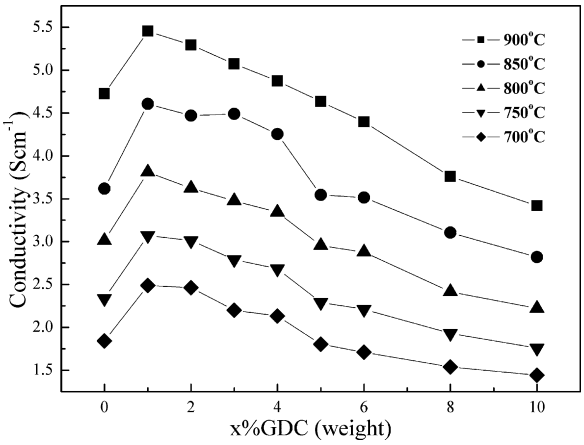

Fig. 7. Effect of the GDC content on the conductivity of the samples in pure H_2 at various temperatures.

LCC + 3 wt.% GDC showed the maximum value at 900 °C. This may be explained by a portion of GDC dissolving into the LCC structure, forming a single phase mixture when the GDC level is below 3 wt.%, leading to a higher electrical conductivity than that of pure LCC. When the GDC content is more than 3 wt.%, which exceeds the solid solubility of GDC in LCC, GDC appears in the grain boundaries. Based on the LCC conduction mechanism under an oxidizing atmosphere, the oxygen vacancy consumes the charge carriers $h^{\bullet}$ resulting in a decrease in electrical conductivity as illustrated by Fig. 4. It can be shown that the appearance of GDC in the LCC grain boundary is a negative for the electrical conductivity, eventually leading to a decrease of total electrical conductivity.

Fig. 7 shows the effect of the GDC content on the conductivity of the samples in pure H_2 at various temperatures. In pure H_2, the electrical conductivity appeared to be higher than that of pure LCC. This can be described by

$$2Ce_{Ce}{}^{\times} + O_O{}^{\times} \leftrightarrow 2Ce'_{Ce} + V_O{}^{\bullet\bullet} + \tfrac{1}{2}O_2\,(g) \quad (7)$$

$$Gd_2O_3 \xrightarrow{CeO_2} 2Gd'_{Ce} + V_O{}^{\bullet\bullet} + 3O_O{}^{\times} \quad (8)$$

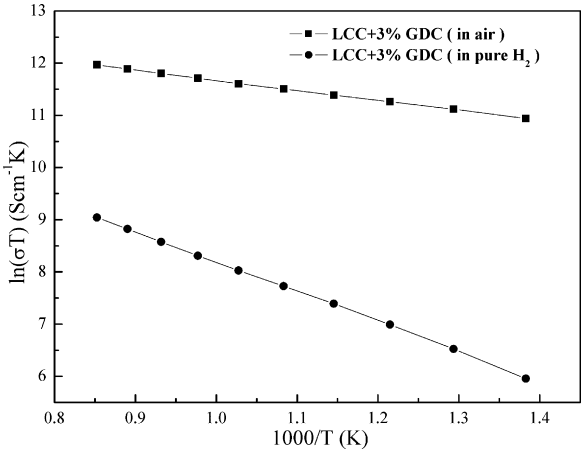

Fig. 8. Total conductivity of LCC + 3 wt.% GDC in air and in H_2 at different temperatures.

where, $Ce_{Ce}^{\times}$ represents Ce-site, Ce'_{Ce} stands for Ce^{4+} on Ce-site and Gd'_{Ce} stands for Gd^{3+} on Ce-site. This indicated that the occurrence of GDC in pure H_2 at high temperature increased the oxygen vacancy concentration. According to reaction (4), in the low oxygen activity regime the increasing of the oxygen vacancy concentration enhanced the $Cr_{Cr}^{\bullet}$ concentration that contributed to larger electrical conductivity. This may be the reason why the electrical conductivity of LCC + 1 wt.% GDC is larger than that of LCC. However, Eq. (5) indicates that if the oxygen vacancy concentration goes up, the $Cr_{Cr}^{\bullet}$ concentration reduces, which leads to the electrical conductivity decrease. As shown in Fig. 7, when the GDC content is more than 2 wt.%, the electrical conductivity gradually decreased.

As mentioned above, the different electrical conductivities in air and in pure H_2 can be explained by different mechanisms: electrical compensation and ionic compensation, respectively. This means that the activation energy E_a for the conduction is different too. From Figs. 4, 6 and 8, it can be calculated that the activation energies are 16.2 kJ mol^{-1} in air and 48.5 kJ mol^{-1} in pure H_2. Moreover, the activation energy E_a appeared to be constant when the GDC ranged from 0 to 10 wt.% either in air or in pure H_2.

From Fig. 8, it can be also seen that the total electrical conductivities of LCC + 3 wt.% GDC in air and in pure H_2 were 134.48 and 5.07 S cm^{-1} at 900 °C, and dropped to 124.56 and 3.48 S cm^{-1} at 800 °C, respectively. Since a value of 1 S cm^{-1} is a well-accepted minimum electrical conductivity for the application of interconnects in SOFCs [29], the currently reported material system has an electrical conductivity adequate for use as an interconnect material for intermediate temperature solid state oxide fuel cells (IT-SOFCs). No sharp changes in activation energy were observed over the temperature range in pure H_2, suggesting that a first-order change did not take place during the process [30]. A conductivity gradient across the doped $LaCrO_3$ is established when it is utilized as an interconnect in a SOFC, considering that it is subjected to fuel on one side and oxidant on the other. Fortunately, the overall conductivity of the doped $LaCrO_3$ is still sufficient for its use as long as the operating temperature is above 800 °C. At temperatures below 800 °C, the electrical conductivity of doped $LaCrO_3$ is reported to experience substantial degradation [31]. This limitation renders it virtually useless for IT-SOFCs operating in the temperature range of 600–800 °C. This is also one of reasons why the operating temperature of the currently explored SOFC should be higher than 800 °C [32]. Luckily in our experiments the addition of GDC improved the electrical conductivity of LCC remarkably, as shown in Figs. 4, 6 and 8, and so solves the problem mentioned above. From the above experimental data it can be concluded that the material system of LCC + GDC is a very promising interconnect material for SOFCs.

3.4. Concern about thermal expansion mismatch

Samples with different GDC contents were pressed into rectangular bars. After firing at 1400 °C for 4 h, these as-prepared rectangular bars were used in a dilatometry test in air. In Fig. 9, the thermal expansion of LCC + 0 wt.% GDC was used as a control. The linear TEC of LCC + 0 wt.% GDC is 11.12 × 10^{-6} K^{-1} in the temperature range of 30–1000 °C. With increasing GDC, the TECs of samples increased and reached the maximum of 14.32 × 10^{-6} K^{-1} when the GDC content is 10 wt.%, suggesting a distinct effect of GDC on the sample's TEC. However, the TECs of most samples are still close to those of other components of an IT-SOFC, such as the YSZ electrolyte, the Sr-doped $LaFeO_3$ cathode and the Ni-SDC or Ni-YSZ anode. Therefore, it would be possible to minimize the thermal stress developed during stack start-up and shutdown.

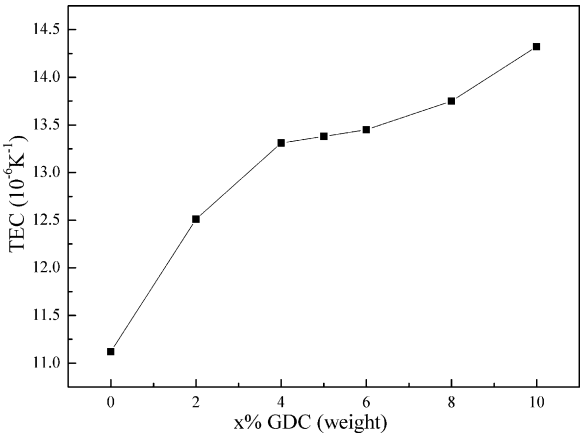

Fig. 9. The TEC of different samples in the temperature range of 30–1000 °C in air.

3.5. Oxygen penetration measurements

Under SOFC operating environments, the interconnect must exhibit excellent electrical conductivity preferably with nearly 100% electronic conduction. This implies that not only the electrical transference number should be high, but also the absolute magnitude of the electrical conductivity should be reasonably large [18]. For our samples the oxygen penetration flux was examined using gas chromatography. The oxygen pressures on the two sides of pellets were 0.000861 and 0.25 atm, respectively.

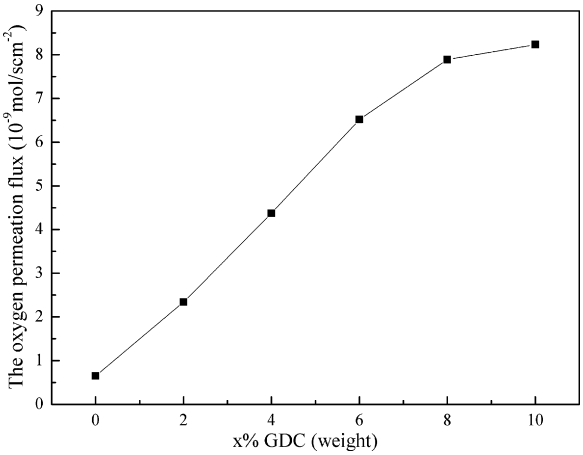

Fig. 10. The influence of the GDC content in LCC + GDC on oxygen permeation flux at 800 °C.

The thickness of pellet was 1.11 mm. The oxygen permeation flux values at 800 °C are shown in Fig. 10. This clearly shows that the oxygen permeation flux increased with increase of GDC content, ranging from 6.51×10^{-10} mol s^{-1} cm^{-2} (of pure LCC) to 8.23×10^{-9} mol s^{-1} cm^{-2} (of LCC + 10 wt.% GDC) at 800 °C. Therefore, this material system exhibits excellent electrical conductivity and a very small oxygen permeation flux. Therefore, it is very promising as an interconnect for intermediate temperature solid oxide fuel cells (IT-SOFC).

4. Conclusion

In the past two decades, many efforts have been devoted to the study of doped lanthanum chromites as an interconnect material for electrolyte-supported planar SOFC. However, little research has been conducted on the composite of LCC and electrolyte. Here, we report a LCC + GDC as an interconnect material for SOFCs. The electrical conductivity of the materials with a 3 wt.% GDC content achieved a maximum of 134.48 S cm^{-1} at 900 °C in air. At 700 and 800 °C, the electrical conductivities also reached 112.84 and 124.56 S cm^{-1} in air, respectively. In pure H_2 the electrical conductivities were 2.20 and 3.48 S cm^{-1}, respectively. At 900 °C in pure H_2, the electrical conductivity reached a maximum of 5.45 S cm^{-1} when the GDC content was 1 wt.%, which is much higher than that of pure LCC. A value of 1 S cm^{-1} is a well-accepted minimum acceptable electrical conductivity for the application of interconnects in SOFCs. At temperatures below 800 °C, the electrical conductivity of doped $LaCrO_3$ decreases substantially, making it virtually useless for SOFCs operating in the temperature range of 600–800 °C, thus it is not feasible to use a doped $LaCrO_3$ as the interconnect material for SOFCs working at lower operating temperatures. However, the LCC + GDC materials system solves this problem very well. With increase of GDC content, the relative density increased, reaching 98.5% when the GDC content was 10 wt.%, and the TEC also increased from 11.12 to 14.32×10^{-6} K^{-1}, showing a high compatibility with the other cell components. Therefore, the LCC + GDC system could be a high-performance interconnect material for reducing the operating temperature of solid oxide fuel cells.

Acknowledgments

This work is supported by the Natural Science Foundation of China under contract no. 50572099. Authors gratefully appreciate and acknowledge the reviewer's critical and constructive comments on the manuscript.

References

[1] N.Q. Minh, J. Am. Ceram. Soc. 76 (3) (1993) 563–588.
[2] H. Yokokawa, N. Sakai, T. Horita, K. Yamaji, Fuel Cells 1 (2) (2001) 117–131.
[3] J.W. Fergus, Solid State Ionics 171 (2004) 1–15.
[4] W.Z. Zhu, S.C. Deevi, Mater. Sci. Eng. A 348 (2003) 227–243.
[5] J.W. Fergus, Solid State Ionics 171 (2004) 1–15.
[6] N. Sakai, T. Kawada, H. Yokokawa, M. Dokiya, J. Mater. Sci. 25 (1990) 4531–4534.
[7] M. Masashi, H. Yoshiko, N.M. Sammes, Solid State Ionics 135 (2000) 743–748.
[8] M. Mori, Y. Hiei, T. Yamamoto, J. Am. Ceram. Soc. 84 (4) (2001) 781–786.
[9] M. Mori, Y. Hiei, J. Am. Ceram. Soc. 84 (11) (2001) 2573.
[10] W.J. Weber, C.W. Griffin, L. Bates, J. Am. Ceram. Soc. 70 (4) (1987) 265–270.
[11] K. Yoshi, J. Solid State Chem. 159 (2001) 204.
[12] N.J. Hess, G.D. Maupin, L.A. Chick, et al., J. Mater. Sci. 29 (1994) 1873.
[13] L.-S. Park, S.-J. Kim, B.-H. Lee, et al., Jpn. J. Appl. Phys. 36 (1997) 6426.
[14] L.A. Chick, L.R. Pederson, G.D. Maupin, et al., Mater. Lett. 10 (1990) 6.
[15] L.A. Chick, G.D. Maupin, G.L. Graff, et al., Mater. Res. Soc. Symp. 249 (1992) 159.
[16] R.E. Juarez, D.G. Lamas, G.E. Lascalaea, et al., J. Eur. Ceram. Soc. 20 (2000) 133.
[17] A. Tsoga, A. Naoumidis, W. Jungen, et al., J. Eur. Ceram. Soc. 19 (1999) 907.
[18] D.B. Meadowcroft, in: T. Gray (Ed.), International Conference on Strontium Containing Compounds, Atlantic Research Institute, Halifax, Canada, 1973, p. 119.
[19] J. Mizusaki, S. Yamauchi, K. Fueki, A. Ishikawa, Solid State Ionics 12 (1984) 119.
[20] D.P. Karim, A.T. Aldred, Phys. Rev. B 20 (1979) 2255.
[21] H.U. Anderson, J.H. Kuo, D.M. Sparlin, in: S.C. Singhal (Ed.), Proceedings of the First International Symposium on Solid Oxide Fuel Cells, PV89-11, The Electrochemical Society Proceedings Series, Pennington, NJ, 1989, p. 111.
[22] B.F. Flandermeyer, M.M. Nasrallah, D.M. Sparlin, H.U. Anderson, High Temp. Sci. 20 (1985) 195.
[23] J.B. Webb, M. Sayer, A. Mansingh, Can. J. Phys. 55 (1977) 1725.
[24] B.K. Flandermeyer, M.M. Nasrallah, A.K. Agarwal, H.U. Anderson, J. Am. Ceram. Soc. 67 (1984) 195.
[25] J. Mizusaki, S. Yamauchi, K. Fueki, A. Ishikawa, Solid State Ionics 12 (1984) 119.
[26] H.E. Hofer, W.F. Kock, J. Electrochem. Soc. 140 (1993) 2889.
[27] I. Yasuda, T. Hikita, J. Electrochem. Soc. 140 (1993) 1669.
[28] D.B. Meadowcroft, Br. J. Appl. Phys. 2 (1969) 1225.
[29] N.Q. Minh, C.R. Horne, F.S. Liu, D.M. Moffatt, P.R. Staszak, T.L. Stillwagon, J.J. S VanAckeren, Proceedings of the 25th Intersociety Energy Conversion Engineering Conference, vol. 13, American Institute of Chemical Engineers, New York, 1990, p. 256.
[30] S. Tao, J.T.S. Irvine, J. Electrochem. Soc. 151 (2) (2004) A252–A259.
[31] B.C.H. Steele, in: J.A.G. Drake (Ed.), Electrochemistry and Clean Energy, Royal Society of Chemistry, 1994, p. 8.
[32] W.Z. Zhu, S.C. Deevi, Mater. Sci. Eng. A 348 (2003) 227–243.